Synthesis of $LaNiCeO_2$ Mixed Oxide with Various *Microcrystalline Cellulose* Templated for Deoxygenation of Waste Cooking Oil

Radhila Widya Putri Octora[1], *Ingelia Yuan* Fernanda[1], *Trias Alzatory* Ersyada[1], *Stella* Jovita[1], *Khawiyatur Riv'ah* Agustina[1], *Mukhamad Rojib* Aminudin[1], *Afifah* Rosyidah[1,*], *Didik* Prasetyoko[1], *Eka Putra* Ramdhani[2] , and *Nurul Asikin* Mijan[3]

[1]Department of Chemistry, Faculty of Science and Data Analytics, Institut Teknologi Sepuluh Nopember (ITS), Sukolilo, Surabaya 60111, Indonesia
[2]Department of Chemistry, Faculty of Engineering and Maritime Technology, Raja Ali Haji Maritime University, Senggarang, Tanjungpinang, 29100, Indonesia
[3]Department of Chemistry, Faculty of Science and Technology, Universiti Kebangsaan Malaysia, 43600 Bangi, Selangor, Malaysia

Abstract. The synthesis of $LaNiCeO_2$ mixed oxides utilizing varying proportions of microcrystalline cellulose (MCC) (12.5%, 25%, and 37.5%) has been successfully achieved. The resulting materials were characterized through XRD, FESEM, N_2 adsorption-desorption isotherms, and TGA-DTG. XRD analysis confirmed that all synthesized $LaNiCeO_2$ mixed oxides exhibited a stable CeO_2 phase. Notably, increasing the MCC content led to an improvement in the catalysts' pore volume and surface area, with the $LaNiCeO_2$-12.5% MCC sample exhibiting a primarily mesoporous structure and minimal micropore contribution. The $LaNiCeO_2$-25% MCC catalyst demonstrated optimal physicochemical properties, indicating its high suitability for catalytic applications. The catalytic deoxygenation of waste cooking oil (WCO) was carried out in a semi-batch reactor at 380 °C for a duration of 4 hours, with a catalyst loading set at 1% of the WCO's weight. The $LaNiCeO_2$-12.5% MCC catalyst exhibited exceptional deoxygenation activity, achieving a 100% conversion, a liquid product yield of 45%, and hydrocarbon selectivity of 98%. The excellent catalytic performance is due to the synergistic interaction between Ni, Ce, and La metals, combined with improved properties that promote the deoxygenation reaction. These results highlight the potential of $LaNiCeO_2$ as an effective catalyst for biofuel production.

* Corresponding author: afifah@chem.its.ac.id

© The Authors, published by EDP Sciences. This is an open access article distributed under the terms of the Creative Commons Attribution License 4.0 (https://creativecommons.org/licenses/by/4.0/).

1 Introduction

Since the beginning of the Industrial Revolution, the excessive use and overexploitation of fossil fuels have significantly worsened the urgent challenge of climate change. In the last hundred years, the average surface temperature of the Earth has increased by approximately 0.8°C, along with a notable rise in sea level of about 18 cm, both of which are directly linked to heightened carbon emissions from the combustion of fossil fuels [1]. Despite considerable efforts to develop renewable energy resources, fossil fuels continue to dominate the global energy landscape, accounting for nearly 80% of total energy consumption [2]. This reality underscores the urgent need for alternative energy sources.

In response to this critical challenge, there has been a growing focus on harnessing biomass—specifically, waste cooking oil (WCO), animal fats, and microalgal oils—as promising renewable alternatives for producing carbon-neutral fuels [3]. However, WCO presents significant challenges for direct utilization as a fuel due to its inherent instability, high viscosity, and low calorific value, primarily attributable to the presence of oxygenated compounds such as carboxyl groups [4], [5]. These characteristics necessitate further processing to enhance its viability, with catalytic deoxygenation emerging as a pivotal method for converting WCO into usable biofuels. This process involves cleaving C-O bonds in oxygenated compounds, optimizing the biofuel's composition, and enhancing its energy density and performance [6]. Effective catalysts are essential in this process to improve reaction activity [4].

Among the various catalysts used, metal oxide-based catalysts have received considerable attention due to their exceptional catalytic activity. Notably, the combination of cerium (Ce), lanthanum (La), and nickel (Ni) has demonstrated exceptional efficacy in deoxygenation processes. Cerium oxide (CeO_2) is particularly distinguished by its superior oxygen storage and release capabilities, owing to its redox transition between Ce^{4+} and Ce^{3+}, rendering it ideal for catalysis and energy storage applications [6], [7]. Lanthanum oxide (La_2O_3) plays a crucial role in facilitating the decarboxylation pathway, effectively eliminating C-O bound species and selectively producing hydrocarbons predominantly within the C15 to C17 range [9]. Nickel-based catalysts, recognized for their cost-effectiveness, provide deoxygenation performance comparable to that of noble metals, with numerous studies underscoring their efficacy in enhancing biofuel production. The synergistic interactions of these mixed oxides present a promising opportunity for enhancing biofuel yields by effectively catalyzing the deoxygenation of waste cooking oil.

However, a prevalent issue with metal oxide-based catalysts is their inherently small pore sizes and surface areas [10]. Consequently, incorporating templates is essential to enhance their physicochemical properties. Nevertheless, the use of synthetic templates often poses environmental concerns and limits scalability for industrial applications due to their high costs. Prior research has shown that ZSM-5 can be effectively synthesized using natural templates obtained from microcrystalline cellulose (MCC), leading to notable enhancements in pore size and surface area [11], [12].

In light of these findings, this research employs biomass-based microcrystalline cellulose as a hard template to enhance the pore size and surface area of mixed metal oxides. Mixed oxides are synthesized with varying MCC template ratios (12.5%, 25%, and 37.5%) to determine the optimal addition and investigate its influence on catalytic activity during WCO deoxygenation. The ultimate goal is to achieve a high liquid yield and hydrocarbon selectivity in the resultant biofuel.

2 Experimental

2.1 Materials

Microcrystalline Cellulose, Cerium (III) nitrate hydrate ($Ce(NO_3)_3 \cdot 6H_2O$, 99%), Lanthanum (III) nitrate hydrate ($La(NO_3)_3.6H_2O$, 99%), and Nickel (II) nitrate hexahydrate ($Ni(NO_3)_2.6H_2O$, 99%), were purchased from Sigma-Aldrich, Germany, Citric acid, Ethanol, Deionized water, Waste cooking oil (WCO) as feedstock.

2.2 Synthesis of $LaNiCeO_2$

The materials were synthesized using the following procedure [13]. A stoichiometric mixture of $Ce(NO_3)_3 \cdot 6H_2O$, $La(NO_3)_3 \cdot 6H_2O$, $Ni(NO_3)_2 \cdot 6H_2O$, and citric acid in a ratio of 1:0.5:0.5:2 was dissolved in 30 ml of ethanol and 10 ml of deionized water. The solution was stirred at room temperature for 12 hours to achieve a homogeneous complex. Subsequently, the solution was dried using a vacuum evaporator at 70 °C. The resulting gel was then placed in an oven at 70 °C for 24 hours. Finally, the dried solid was calcined in a muffle furnace at 300 °C for 4 hours.

2.3 Characterization of Catalysts

The crystal structure of the catalyst was characterized using X-ray diffraction (XRD) with a PHILIPS-binary X'Pert MPD apparatus (30 mA, 40 kV) over a 2θ range of 5° to 100°. Fourier Transform Infrared (FTIR) measurements were performed using a Shimadzu Instrument Spectrum One 8400S in the range of 4000 to 400 cm^{-1}. The catalyst's morphology was examined using Field Emission Scanning Electron Microscopy (FESEM), while Energy Dispersive X-Ray (EDX) analysis was conducted to determine the elemental composition of the materials. The surface area was assessed by the Brunauer-Emmett-Teller (BET) method to evaluate N_2 adsorption-desorption. Pore size distribution and pore volume were calculated using the BJH method. Thermal analysis was conducted via TGA using a Hitachi STA7200 Simultaneous Thermal Analyzer across varying temperatures. Finally, pore properties were analyzed using Transmission Electron Microscopy (Hitachi HR-9500 TEM), with the resulting TEM images processed using ImageJ to determine pore size.

2.4 Catalytic deoxygenation reaction of WCO

The deoxygenation of waste cooking oil (WCO) was conducted in a semi-batch reactor under a nitrogen atmosphere. The catalyst was utilized at 380 °C, with a catalyst loading of 1% relative to the weight of WCO. The catalyst was mixed with the WCO in a three-necked round-bottom flask and stirred continuously for 4 hours. Liquid products were sampled hourly and collected in a separate flask for analysis using GC-MS. The conversion of WCO and the liquid yield were calculated using Equations (1) and (2), respectively.:

$$\%\text{Conversion} = \frac{(\text{wo WCO - WCOwt})}{\text{wo WCO}} \times 100\% \quad (1)$$

$$\%\text{Liquid yield} = \left(\frac{\text{weight of deoxygenated liquid}}{\text{wo WCO}}\right) \times 100\% \quad (2)$$

2.4 GC-MS analysis for deoxygenated liquid product

The liquid products of the deoxygenation reaction were analyzed using gas chromatography-mass spectrometry (HP 6890 GC). The capillary column used was HP-5MS, with dimensions of 30 m in length, 0.25 mm in inner diameter, and a film thickness of 0.25 μm. 1-Bromohexane served as the internal standard for quantitative analysis. The selectivity of hydrocarbons was calculated using Equation (3), while the concentrations of liquid products such as carboxylic acids, alcohols, aldehydes, paraffins, olefins, and others were determined using Equation (4).

$$\%\text{Selectivity hydrocarbon} = \frac{(\text{peak area of desired hydrocarbon})}{(\text{peak area of total hydrocarbon})} \times 100\% \quad (3)$$

$$\%\text{Selectivity} = \frac{(\text{peak area of organic product})}{(\text{total area of liquid product})} \times 100\% \quad (4)$$

3 Result and discussion

3.1 Characterization of Material

3.1.1 X-Ray diffraction (XRD) analysis

The X-ray diffraction (XRD) patterns of the synthesized $LaNiCeO_2$ mixed oxide samples with varying amounts of microcrystalline cellulose (MCC) are presented in Fig. 1. All samples exhibit characteristic peaks corresponding to CeO_2 (JCPDS No. 34-0934) at diffraction angles (2θ) of 27.8°, 32.3°, 46.65°, and 55.27°, which can be indexed to the (1 1 1), (2 0 0), (2 2 0), and (3 1 1) crystal planes, respectively. These peaks indicate the presence of cubic CeO_2 across all samples [14]. The XRD pattern reveals a slight shift in peak positions, indicating alterations in the crystal lattice resulting from the doping process. This shift in peak position suggests changes in interplanar spacing. The incorporation of La^{3+} ions into the lattice appears to occur through a substitution mechanism at the sites of Ce^{3+} ions, leading to lattice expansion due to the size difference between La^{3+} (1.06 Å) and Ce^{3+} (1.02 Å)[15].

As the MCC content increases from 12.5% to 37.5%, there is a slight broadening of the diffraction peaks, particularly 37.5% MCC, which may indicate a decrease in crystallite size or an increase in structural disorder. This broadening suggests that higher MCC content could potentially introduce more defects or promote smaller crystallites during the synthesis of $LaNiCeO_2$ mixed oxides. The absence of significant shifts in peak positions suggests that the $LaNiCeO_2$ structure remains stable and that increasing MCC content does not lead to phase transformation or the formation of new crystalline phases. Furthermore, the relative intensities of the diffraction peaks show a slight decrease with increasing MCC content. This reduction may be attributed to the dispersion of CeO_2 crystallites or an increase in the amorphous phase introduced by the presence of MCC.

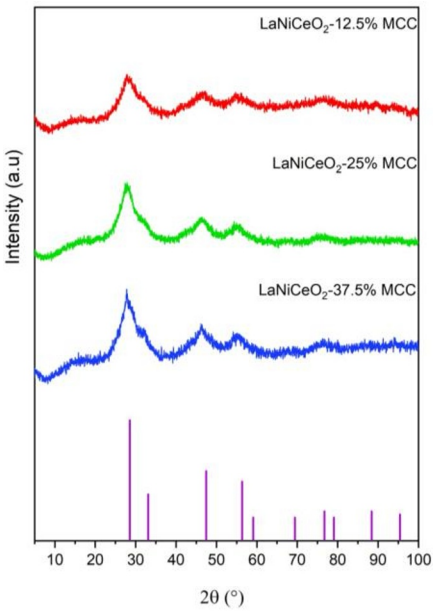

Fig. 1. XRD pattern of La_0NiCeO_2 with variation microcrystallile cellulose templated and JCPDS data of CeO_2 (No.34-0394)

3.1.2 Nitrogen adsorption-desorption isotherms

The nitrogen adsorption-desorption isotherms for the $LaNiCeO_2$ mixed oxide catalysts with varying amounts of microcrystalline cellulose (MCC) are illustrated in Fig. 2, while the specific surface area and pore distribution values are provided in Table 1. Based on IUPAC classification, all $LaNiCeO_2$ oxide mixtures exhibit type IV isotherms accompanied by H3 hysteresis loops, which confirm the presence of mesoporous structures. The H3 hysteresis loop typically indicates slit-like pores and is associated with materials that have irregular or non-uniform pore structures, which in this case is likely due to the use of MCC as a hard template during the synthesis process [13]. At a relative pressure (P/P_0) of less than 0.3, nitrogen filling occurs, forming the first monolayer. When the relative pressure exceeds 0.4, hysteresis loop formation occurs, indicating capillary condensation with a small amount of nitrogen adsorbed in the mesopores of the catalyst.

Table 1 displays the surface area of the materials, as determined using the BET method. From the data it can be known that the $LaNiCeO_2$-25% MCC sample has the highest surface area (52.36 m^2/g), followed by the 37.5% MCC sample (46.62 m^2/g), and the 12.5% MCC sample (36.00 m^2/g). This trend suggests that the introduction of MCC as a template increases the surface area, with the optimal amount (25%). The total pore volume, calculated from the DFT method, shows that the $LaNiCeO_2$-25% MCC sample has the highest mesopore volume (0.069 cc/g) and a notable micropore volume (0.011 cc/g). The 37.5% MCC sample has a slightly higher total pore volume (0.076 cc/g), while the 12.5% MCC sample exhibits the smallest total pore volume (0.064 cc/g). The micropore contribution is minimal in the 12.5% MCC sample, reflecting a mostly mesoporous structure. The average pore size across the samples ranges from 3.85 to 3.94 nm, indicating that all catalysts fall within the mesoporous range. The slight differences in pore size suggest that the pore structure remains relatively consistent across varying MCC content, but overall porosity is enhanced as the MCC content increases.

Table 1. Physicochemical properties of $LaNiCeO_2$

Catalyst	Surface Area (m^2/g)			Pore Volume (cc/g)			[a]Pore size (nm)
	[a]S_{BET}	[b]S_{meso}	[c]S_{micro}	[b]V_{meso}	[c]V_{micro}	V_{total}	
$LaNiCeO_2$-12.5% MCC	36.00	32.16	35.75	0.064	0.000	0.064	3.85
$LaNiCeO_2$-25% MCC	52.36	47.50	34.98	0.069	0.011	0.080	3.94
$LaNiCeO_2$-37.5% MCC	46.62	43.70	33.01	0.065	0.011	0.076	3.92

[a] Surface Area and Pore size calculated by BET analysis
[b]Surface area mesopore and volume mesopore were calculated from DFT method
[c]Surface area micropore and volume micropore were calculated from t-plot method

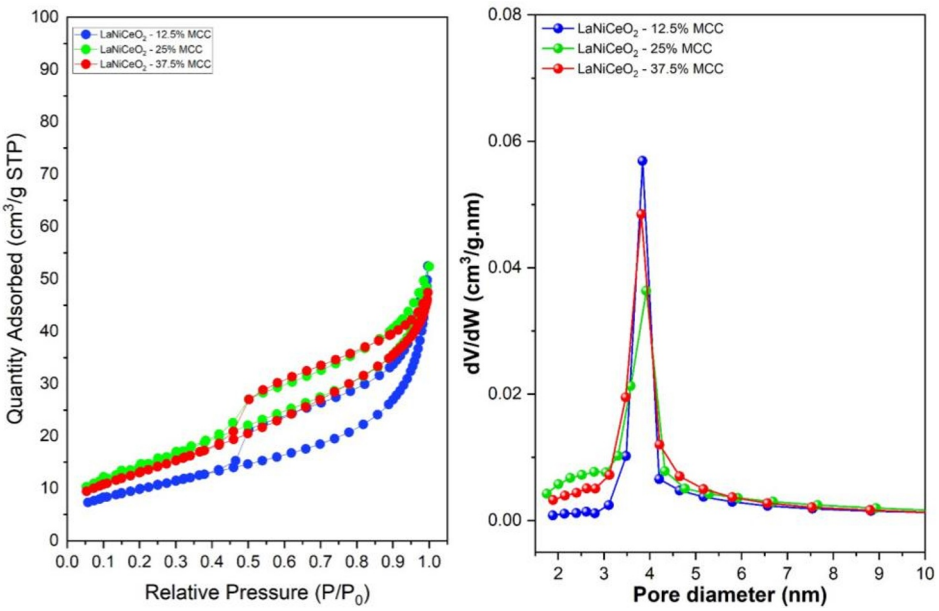

Fig. 2. Isoterm physisorp and pore size distribution of $LaNiCeO_2$

3.1.3 FESEM-EDX

Field-Emission Scanning Electron Microscopy (FE-SEM) analysis was conducted to examine the microstructure and morphology of $LaNiCeO_2$ mixed oxides with different amounts of added MCC, as shown in Fig. 3. By increasing the magnification up to 1 µm. The microscopic view shows that all samples have micrometer-sized multidirectional crystals that are heterogeneous in shape with some agglomerations [16]. The result also revealing a porous and highly rough surface with a significant number of cavities and voids. The EDX spectrum confirms the presence of La, Ni, Ce, and O, indicating that the elements are well-distributed across the sample.

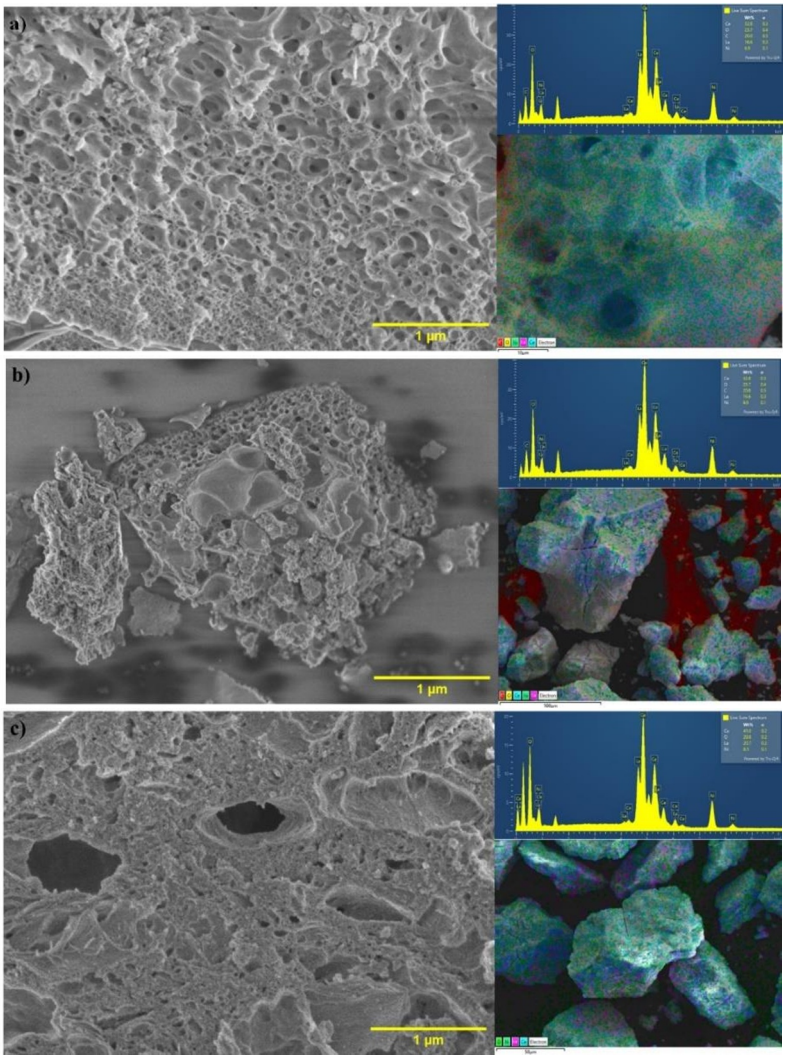

Fig. 3. FESEM analysis of a) $LaNiCeO_2$-12.5% MCC, b) $LaNiCeO_2$-25% MCC, dan c) $LaNiCeO_2$-37.5% MCC

3.1.3 TGA-DSC analysis

Thermogravimetric analysis (TGA) of $LaNiCeO_2$ with varying MCC compositions offers insights into its thermal stability and degradation mechanisms. The analysis was carried out from room temperature to 1000°C, measuring weight loss, heat flow, and the overall decomposition behavior.

In general, samples 12.5 and 37.5% MCC show 3 decompositions which are related to the removal of physical water and crystal water, nitrate decomposition, and citric acid decomposition. Then, phase formation occurs at high temperature. Meanwhile, the 25% of MCC have 2 decompositions. All samples show initial weight loss between 50-200°C and exhibit endotermic peak in DSC profile. The significant weight loss between 200-400 °C that the exothermic reaction is associated with nitrate decomposition which is release NO_x and

oxygen. At temperature 400-600°C is exothermic process to formation of oxide. Then, the phase formation occurs at temperature 600-800°C [17].

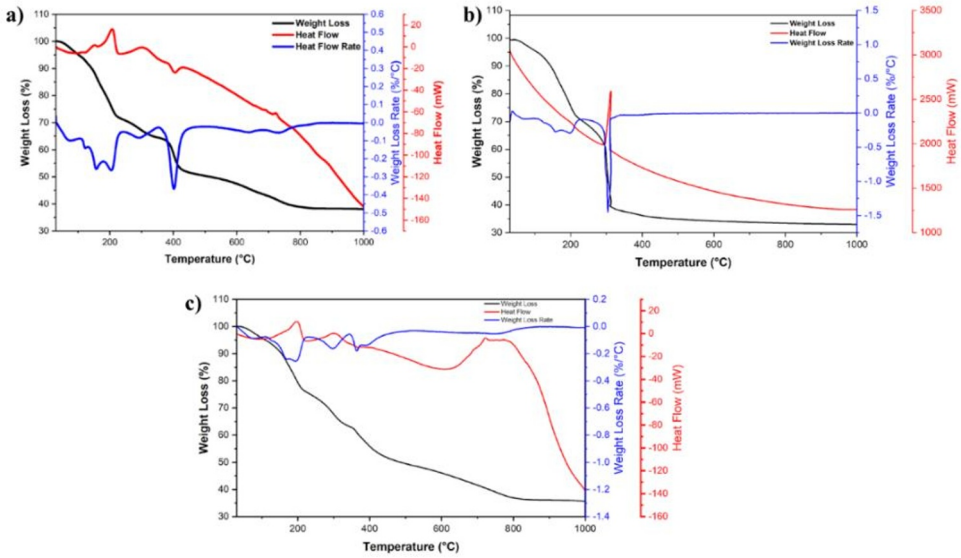

Fig. 4. TGA-DSC Analysis of a) $LaNiCeO_2$-12.5% MCC, b) $LaNiCeO_2$-25% MCC, dan c) $LaNiCeO_2$-37.5% MCC

3.1.3 Catalytic deoxygenation of WCO

The deoxygenation of waste cooking oil was conducted using $LaNiCeO_2$ catalysts with different MCC contents. The reaction was performed in a semi-batch reactor featuring a digital heating mantle, magnetic stirrer, thermometer, condenser, and vacuum setup. A catalyst loading of 1%wt relative to the WCO was employed. The process was carried out at 380°C for 4 hours under a nitrogen flow. The resulting liquid products were then analyzed using GC-MS.

In Fig 5a, all catalysts are active for the conversion of waste cooking oil. Every catalyst obtained 100% conversion. Previous research [18] shows the algal HO conversion also reach 100% with lanthanum catalyst. These catalyst produce a liquid product (45-33%). Liquid product yield decreased in the following order $LaNiCeO_2$-12.5% MCC > $LaNiCeO_2$-25% MCC > $LaNiCeO_2$-37.5% MCC. Among all the catalyst, $LaNiCeO_2$-12.5% MCC showed the highest yield (45%). This may be due to the larger mesopore volume [10]. The volume ratio of mesopores and micropores of this catalyst is largest than that of the others. Mesoporosity increases the diffusivity of reactant and product by providing transportation for efficient mass transfer during deoxygenation [19].

Fig 5b showed that the catalyst also produces oxygenated intermediate products (carboxylic acid, alcohol and ketone) and non-oxygenated compound (hydrocarbon, cyclic and aromatic). All catalyst have a high hydrocarbon selectivity. $LaNiCeO_2$-12.5% MCC has the highest hydrocarbon yield of 98%. Then, catalyst 37.5, 25 % of MCC were 94 and 90%, respectively. This indicates that the catalyst is very effective in promoting deoxygenation activity. Similar findings were reported by Khalit [20], who obtained a hydrocarbon yield of 89% with the use of nickel on the support. Previous research with Ni-Ce bimetals showed that the presence of cerium oxide contributes a large catalytic activity [21].

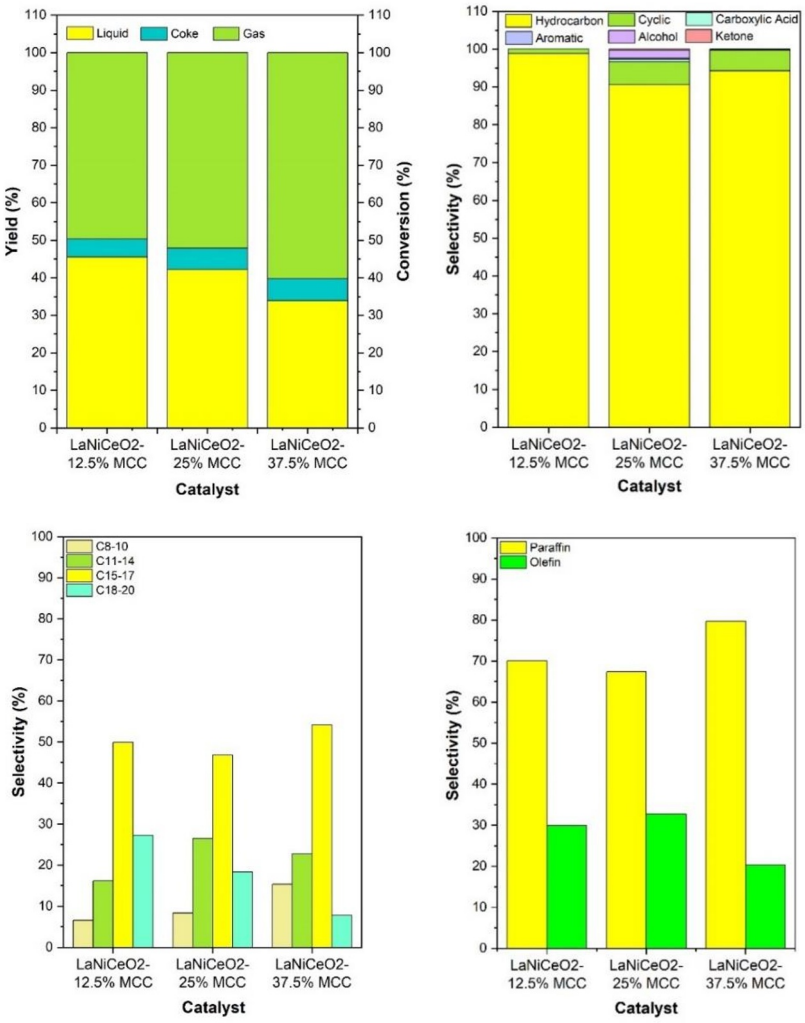

Fig. 5. a) Yield Liquid, b) Product Selectivity, c) Carbon Selectivity, dan d) Hydrocarbon selectivity of various catalyst

Fig 5.c summarizes the hydrocarbon fraction. All catalysts show the highest distribution of hydrocarbon fractions at C_{15}-C_{17}. This is due to decarboxylation and decarbonylation reactions. This decarboxylation and decarbonylation reduces 1 carbon chain by removing CO_2 or CO [22]. C_{15} and C_{17} fraction is compared to the FFA components of WCO, where the main components are oleic acid ($C_{18:1}$) and palmitic acid ($C_{16:0}$) which undergoes the DCO/DCO_2 reaction [10],[19].

Figure 5.d shows the distribution of paraffins and olefins. The catalyst exhibits higher paraffin selectivity compared to olefins. The higher distribution of paraffins (alkanes) indicates that the dominant reaction pathway is decarboxylation [23]. This highlights the catalyst's role in facilitating the decarboxylation reaction. The increased paraffin/olefin ratio is attributed to hydrogenation, which occurs as a result of the reaction between CO and H_2O in the water-gas shift reaction (WGSR) [19].

4 Conclusion

In conclusion, $LaNiCeO_2$ mixed oxides were successfully synthesized using microcrystalline cellulose (MCC) as a template. XRD analysis verified the presence of a stable CeO_2 phase in all samples, with higher MCC content leading to a reduction in crystallite size. The increase in MCC also improved the surface area and pore volume, enhancing the overall catalytic performance. The $LaNiCeO_2$-12.5% MCC catalyst demonstrated excellent activity in deoxygenating waste cooking oil (WCO) into biofuel, achieving 100% conversion, 45% liquid product yield, and 98% hydrocarbon selectivity. This superior performance is due to the combined effects of Ni, Ce, and La metals, along with the increased pore volume, making these materials promising catalysts for biofuel production.

Acknowledgement

The authors would like to acknowledge the Kemendikbud RISTEKDIKTI with contract No 1818/ PKS/ITS/2024 for the financial support under PTM research grant.

References

1. M. Xu, Z. Shi, X. Zhu, Y. Lai, A. Xia, Y. Huang, X. Jiang, J. He, M. Zhou, X. Zhu, and Q. Liao, International Journal of Hydrogen Energy **52**, 83 (2024)
2. Z. Bian, Z. Wang, B. Jiang, P. Hongmanorom, W. Zhong, and S. Kawi, Renewable and Sustainable Energy Reviews **134**, 110291 (2020)
3. A. I. Tsiotsias, S. Hafeez, N. D. Charisiou, S. M. Al-Salem, G. Manos, A. Constantinou, S. AlKhoori, V. Sebastian, S. J. Hinder, M. A. Baker, K. Polychronopoulou, and M. A. Goula, Renewable Energy **206**, 582 (2023)
4. L. K. H. Pham, T. T. V. Tran, S. Kongparakul, P. Reubroycharoen, S. Karnjanakom, G. Guan, and C. Samart, Fuel Processing Technology **185**, 117 (2019)
5. S. Jovita, H. Holilah, N. N. Khairunisa, H. Bahruji, R. E. Nugraha, N. A. Sholeha, A. Aziz, R. Ediati, A. A. Jalil, and D. Prasetyoko, Case Studies in Chemical and Environmental Engineering **10**, 100935 (2024)
6. F. Jin, Y. Yan, and G. Wu, Catalysis Today **355**, 148 (2020)
7. P. A. Periasamy, B. Saravanakumar, J. Johnson William, N. Karthikeyan, and S. Vadivel, Electrochimica Acta **507**, 145144 (2024)
8. T. Montini, M. Melchionna, M. Monai, and P. Fornasiero, Chemical Reviews **116**, (2016)
9. A. Alsultan, N. Mijan, G. Mustafa-Alsultan, H. Lee, K. Wilson, and Y. H. Taufiq-Yap, RSC Advances **10**, (2020)
10. X. Y. Ooi, W. Gao, H. C. Ong, H. V. Lee, J. C. Juan, W. H. Chen, and K. T. Lee, Renewable and Sustainable Energy Reviews **112**, 834 (2019)
11. X. Li, H. Fu, S. Shao, and Y. Cai, Fuel Processing Technology **248**, 107815 (2023)
12. M. Qian, Y. Zhao, E. Huo, C. Wang, X. Zhang, X. Lin, L. Wang, X. Kong, R. Ruan, and H. Lei, Journal of Analytical and Applied Pyrolysis **166**, 105624 (2022)
13. Y. Ruan, Y. Zhao, Y. Lu, D. Guo, Y. Zhao, S. Wang, and X. Ma, Microporous and Mesoporous Materials **303**, 110278 (2020)
14. L. Wang, N. Zhao, X. Yin, W. Wang, Y. Zhao, Z. Zheng, S. Li, J. Wang, and Y. Chen, Fuel **356**, 129444 (2024)
15. A. Rianjanu, K. D. P. Marpaung, C. Siburian, S. A. Muhtar, N. I. Khamidy, J. Widakdo, N. Yulianto, R. Aflaha, K. Triyana, and T. Taher, Results in Engineering **23**, 102748 (2024)

16. K. K. F. Barbosa, D. Aristizábal-Giraldo, J. M. Osorio-Guillén, J. J. S. Acuña, and F. F. Ferreira, RSC Mechanochem. **1**, 69 (2024)
17. D. Çoban Özkan, A. Türk, and E. Çelik, J Mater Sci: Mater Electron **31**, 22789 (2020)
18. M. J. Nuhma, H. Alias, M. Tahir, and A. A. Jazie, Molecules **27**, 6527 (2022)
19. R. E. Nugraha, H. Purnomo, A. Aziz, H. Holilah, H. Bahruji, N. Asikin-Mijan, S. Suprapto, Y. H. Taufiq-Yap, A. A. Jalil, H. Hartati, and D. Prasetyoko, South African Journal of Chemical Engineering **49**, 122 (2024)
20. W. N. A. W. Khalit, N. Asikin-Mijan, T. S. Marliza, M. S. Gamal, M. R. Shamsuddin, M. I. Saiman, and Y. H. Taufiq-Yap, Biomass and Bioenergy **154**, 106248 (2021)
21. N. Aliana-Nasharuddin, N. Asikin-Mijan, G. Abdulkareem-Alsultan, M. I. Saiman, F. A. Alharthi, A. A. Alghamdi, and Y. H. Taufiq-Yap, RSC Adv **10**, 626 (n.d.)
22. K. B. Baharudin, Y. H. Taufiq-Yap, J. Hunns, M. Isaacs, K. Wilson, and D. Derawi, Microporous and Mesoporous Materials **276**, 13 (2019)
23. R. Tamim, D. Prasetyoko, S. Jovita, Y. L. Ni'mah, R. E. Nugraha, H. Holilah, H. Bahruji, R. Yusop, N. Asikin-Mijan, A. A. Jalil, H. Hartati, and D. D. Anggoro, Renewable Energy **232**, 121135 (2024)